Transient Noise and Gain Characterization for Pulse-Operated LNAs

Citation for the original published paper (version of record):
Zeng, Y., Stenarson, J., Sobis, P. et al (2024). Transient Noise and Gain Characterization for Pulse-Operated LNAs. IEEE Microwave and Wireless Technology Letters, 34(7): 911-914.
http://dx.doi.org/10.1109/LMWT.2024.3398248

(article starts on next page)

Transient Noise and Gain Characterization for Pulse-Operated LNAs

Yin Zeng, *Graduate Student Member, IEEE*, Jörgen Stenarson, *Member, IEEE*, Peter Sobis, and Jan Grahn, *Senior Member, IEEE*

***Abstract*— We propose a novel method for direct characterization of transient noise and gain for a pulsed low-noise amplifier (LNA) with nanosecond resolution over a wide bandwidth. The method used a standard noise source and an oscilloscope to measure the time-domain output waveform of the LNA. Transient noise and gain of a gate-pulse-operated C-band LNA at two biases were measured with 50-ns resolution. The method showed good agreement with static measurements. The transient gain was compared with transient S-parameter and drain current measurements, which confirmed the proposed method.**

***Index Terms*— Low-noise amplifier (LNA), noise figure, noise measurement, transients.**

I. Introduction

THE transient noise and gain performance of pulsed low-noise amplifiers (LNAs) is critical for switch-sensitive systems. In a pulsed radar system, receiver LNAs are switched on and off to prevent damage from the high-power transmitter [1], [2]. In a superconducting quantum computer, the average power consumption could be reduced by pulsed operation of the LNAs, and observing its impact on the quality of qubit readout would be of interest. Since the operating window for both the applications are at the sub-microsecond level and highly sensitive to noise, it is important to accurately characterize the transient noise and gain of pulse-operated LNAs at the nanosecond scale.

There are a number of previous studies estimating time-domain recovery of low-noise devices. Most studies in the literature focus on measuring nonlinear response under large-signal injection [3], [4], [5], [6], [7], [8], [9], [10], [11], [12], [13], [14]. The drain current I_D transient was used as an indirect way to estimate the recovery time of the LNA or transistor [10], under the assumption that small-signal performance was spontaneously and linearly dependent on dc behavior [5]. Small-signal gain transients recorded by a high-speed vector network analyzer (VNA) are another method to evaluate the recovery progress of the LNA subject to large-signal pulse interference [9], [12], [13]. However, when the noise temperature is extremely low and critical for overall system performance such as in qubit readout, it is important to also directly characterize the recovery of noise performance. A more direct method is to study the output power in time domain [3], [6], [8] using a power detector and an oscilloscope at the LNA output. However, the envelope recorded by the oscilloscope lost frequency-domain information and made quantitative analysis difficult. A more analytical transient noise analysis was made by evaluating the power spectral density (PSD) in the time domain acquired by a wideband IF (200 MHz) VNA [14]. However, no direct method to quantify the transient noise of the LNA over time was reported.

In this work, we proposed and verified a direct method to quantitatively characterize the transient small-signal noise and gain in a pulsed LNA with nanosecond resolution over a wide bandwidth. The method used an oscilloscope to capture the output waveform of the LNA. Noise and gain were extracted through PSD analysis. The method was tested on a gate-pulsed C-band InP HEMT LNA at two dc biases. The method was validated by comparison with VNA-measured transient gain and I_D of the pulsed LNA.

II. Characterization Method

The proposed setup for LNA noise and gain transient characterization is shown in Fig. 1. An HP346B noise source with around 15-dB excess noise ratio was mounted at the input of the device under test (DUT) whose gate was pulse-operated by a Keysight 33500B arbitrary waveform generator (AWG). Following a 3.1–8.4-GHz bandpass filter and a dc block, the output of the DUT was connected to a Keysight UXR0334A oscilloscope. The oscilloscope had a maximum of 1.56-ms memory depth when operated at 128-GSa/s sampling speed with 33-GHz bandwidth. The DUT drain-bias voltage was static and the transient in I_D was monitored by a Tektronix TCP300 Hall-effect current probe with 100-MHz bandwidth connected to the oscilloscope.

The characterization procedure is described in Fig. 2. Before the measurements, the noise source was either in "ON" or "OFF" state. The gate voltage was then pulsed from a pinch-off quiescent point to an operation point where the DUT is turned on. The oscilloscope captured the transient output waveform

Manuscript received 9 February 2024; revised 12 April 2024; accepted 4 May 2024. Date of publication 21 May 2024; date of current version 9 July 2024. This work was supported in part by Sweden's Innovation Agency (Vinnova) in the Strategic Innovation Program Smartare Elektroniksystem and in part by WiTECH Centre at Chalmers University of Technology. *(Corresponding author: Yin Zeng.)*

Yin Zeng and Jan Grahn are with the Department of Microtechnology and Nanoscience (MC2), Chalmers University of Technology, 412 96 Göteborg, Sweden (e-mail: yzeng@chalmers.se; jan.grahn@chalmers.se).

Jörgen Stenarson is with the Low Noise Factory AB, 412 63 Göteborg, Sweden (e-mail: stenarson@lownoisefactory.com).

Peter Sobis is with the Department of Microtechnology and Nanoscience (MC2), Chalmers University of Technology, 412 96 Göteborg, Sweden, and also with the Low Noise Factory AB, 412 63 Göteborg, Sweden (e-mail: sobis@lownoisefactory.com).

Color versions of one or more figures in this letter are available at https://doi.org/10.1109/LMWT.2024.3398248.

Digital Object Identifier 10.1109/LMWT.2024.3398248

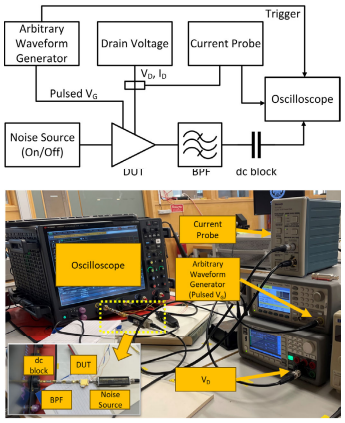

Fig. 1. Schematic and real test environment of the proposed transient noise and gain characterization setup for the pulse-operated LNA.

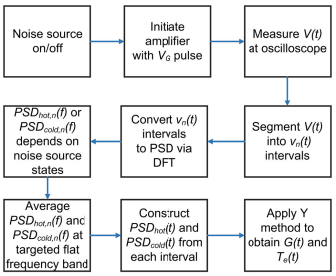

Fig. 2. Flowchart of the proposed noise- and gain-transient characterization method.

$V(t)$ of the DUT. The $V(t)$ was time-segmented into intervals with a window length of targeted time resolution here denoted as $v_n(t)$, where n represents the nth time segment. The $v_n(t)$ should be short enough to have small amplitude change to be assumed to be quasi-time-invariant, whereas sampling points should be sufficient in number to provide adequate frequency resolution and signal-to-noise ratio [14] after discrete Fourier transform (DFT). The PSD at each time step could then be acquired by applying DFT to each time segment. With the noise source in "ON" and "OFF" states, we acquired $\mathrm{PSD}_{\mathrm{hot},n}(f)$ and $\mathrm{PSD}_{\mathrm{cold},n}(f)$, respectively. Under the assumption that the in-band noise and gain of DUT were flat, averaging could be used for the targeted frequency band at each time segment to overcome the random property in the noise measurement [15]. The representative frequency band PSD over time could be acquired as $\mathrm{PSD}_{\mathrm{hot}}(t)$ and $\mathrm{PSD}_{\mathrm{cold}}(t)$. Finally, we could apply the Y method [16] to the "hot" and "cold" pair of PSD to produce the time-domain equivalent noise temperature $T_e(t)$ and gain $G(t)$.

III. Measurement Results

The DUT tested in this work was a 4-8-GHz InP HEMT LNA [17] with reduced gate-bias capacitor to enable faster pulsed operation. Two pulsed gate-voltage V_G bias conditions of the LNA, -92 and -244 mV, were tested with the same fixed drain voltage $V_D = 1.35$ V. The static noise and gain measurements for both the biases are shown in Fig. 3. When V_G was biased at -92 mV, the average noise temperature was 36.8 K and the average gain 41.1 dB over 5–7 GHz. The

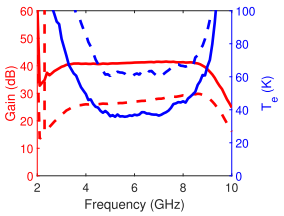

Fig. 3. Measured noise and gain of the tested LNA using static biases. The solid line represents $V_G = -92$ mV and dashed line $V_G = -244$ mV, using the same V_D bias of 1.35 V.

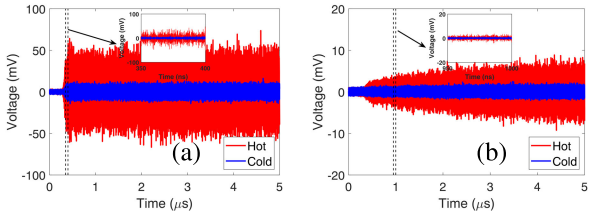

Fig. 4. Output oscilloscope waveform. The insert is a zoom-in with 50-ns time span. (a) $V_G = -92$ mV. (b) $V_G = -244$ mV.

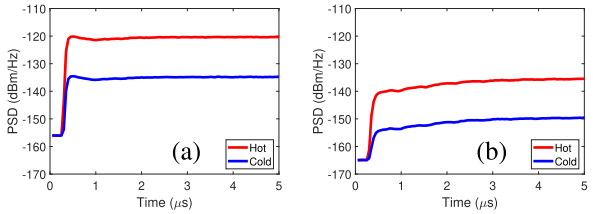

Fig. 5. Hot and cold PSD averaged across 5–7 GHz over 150 pulses for (a) $V_G = -92$ mV and (b) $V_G = -244$ mV over time.

$V_G = -244$-mV bias of the LNA showed 62.0-K average noise temperature and 27.0-dB average gain for the same bandwidth.

The pulse period in this test was set to be 100 μs under 50% duty cycle square wave with the quiescent gate voltage to pinch off the LNA set to -500 mV. The gate pulse rise times for both the biases from the AWG were 15 ns. The time resolution window was set to 50 ns. The first 5 μs of the output waveform versus time for both the biases are plotted in Fig. 4. For $V_G = -92$ mV, the voltage amplitude is seen to rapidly recover to quasi-steady state within 0.5 μs. In contrast, the $V_G = -244$-mV case recovered its amplitude after 4 μs. Both the inserts of Fig. 4 show that within the 50-ns time window, the amplitude change is relatively small and thus can be assumed to be quasi-time-invariant.

After applying DFT to each windowed time segment, the 64-GHz bandwidth PSD was acquired with 15.625-MHz frequency resolution. The bandwidth of the oscilloscope and bandpass filter used in the setup further limited the frequency range to 3.1–8.4 GHz. Under the assumption of a flat in-band frequency response of the LNA, we averaged the PSD over 5–7 GHz to overcome the random fluctuation in the noise measurement. Moreover, 150 pulses were used for averaging the data for the same reason.

Fig. 5 presents the averaged PSD with either "cold" or "hot" noise source. From Fig. 5(a), both the "cold" and "hot" PSD recovered within 0.5 μs with an overshoot for $V_G = -92$ mV, which agreed with the observation from the waveform in Fig. 4(a). In contrast, when biased with $V_G = -244$ mV, both "hot" and "cold" PSD increased rapidly during the first

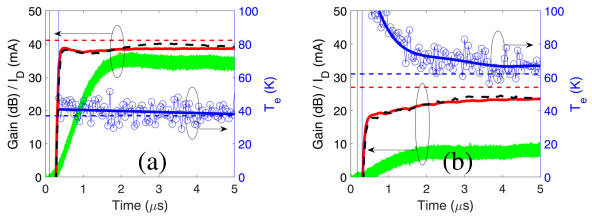

Fig. 6. Calculated transient noise and gain over time in steps of 50 ns for (a) $V_G = -92$ mV and (b) $V_G = -244$ mV. Blue circles represent calculated raw noise temperature, blue solid line is the polynomial curve-fitting of raw noise temperature after the PSD recovers above the noise floor, and blue dashed line represents static measured noise temperature. Red solid line represents calculated gain, black dashed line the gain recovery measured by PNA-X at 6 GHz, and red dashed line the static measured gain. The green line represents I_D over time.

0.5 μs but did not recover to quasi-steady state until 3.5 μs, shown in Fig. 5(b). The PSD noise floor of the oscilloscope was -156.6 and -165.7 dBm/Hz for $V_G = -92$ mV and $V_G = -244$ mV, respectively. This difference between the two bias cases is due to the quantization noise difference in the oscilloscope horizontal scale setting.

Based on the 5–7 GHz and 150 pulses averaged "hot" and "cold" PSD over time in Fig. 5, the noise and gain over time can be calculated by the Y method [16]. The Y factor can be expressed by

$$Y(t) = \frac{\mathrm{PSD_{hot}}(t)}{\mathrm{PSD_{cold}}(t)}. \tag{1}$$

$T_e(t)$ and $G(t)$ of the DUT can be calculated by

$$T_e(t) = \frac{T_{\mathrm{hot}} - Y(t) \times T_{\mathrm{cold}}}{Y(t) - 1} \tag{2}$$

and

$$G(t) = \frac{\mathrm{PSD_{hot}}(t) - \mathrm{PSD_{cold}}(t)}{(T_{\mathrm{hot}} - T_{\mathrm{cold}}) \times k_B} \tag{3}$$

where T_{hot} and T_{cold} are the noise-source equivalent temperatures when turned on and off, respectively. k_B is Boltzmann's constant.

The calculated transient noise temperature and gain are illustrated in Fig. 6. The setup is calibrated by the Y-factor method and reached results consistent to the results done by noise figure analyzer when the LNA is biased under static conditions. The results are compared with the gain acquired by a PNA-X at 6 GHz with 15-MHz IF bandwidth and 50-ns time resolution [13] and I_D transient monitored by the Hall effect current probe [10]. For $V_G = -92$ mV in Fig. 6(a), the gain recovers rapidly within first 0.5 μs with an overshoot, which is indicated by the PSD over time and agrees well with the PNA-X measured gain transient. The calculated raw noise data still exhibited some fluctuations, which can be improved by more data averaging [18]. The polynomial fit noise curve in Fig. 6(a) recovers to 45 K within 0.5 μs and decreases slowly down to 41 K at 5 μs. The decrease in the noise temperature after recovery to quasi-steady states can be critical to noise-sensitive applications such as qubit readout [19]. In contrast, the gain recovery curve can be less sensitive to indicate such a slight change in noise temperature. The I_D stabilizes at 35 mA after 2 μs, which is slower compared with the RF performance recovery in the $V_G = -92$-mV

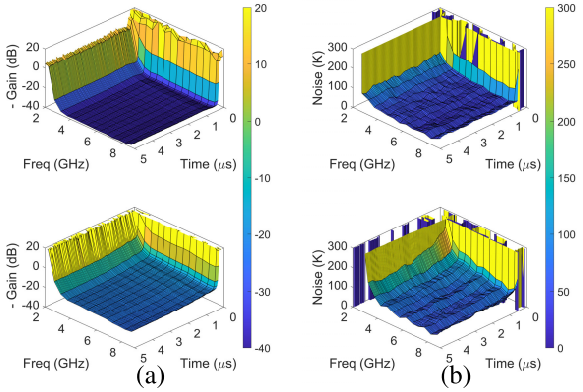

Fig. 7. Three-dimensional plot of (a) negative gain and (b) noise transient in time and frequency domains. Top row: $V_G = -92$ mV and bottom row: $V_G = -244$ mV. Each frequency point averaged 0.5-GHz nearby bandwidth PSD.

case. This could be due to the saturation of gain and noise parameters with increased current bias for the HEMT [20]. This is supported by the results shown in Fig. 6(b), for $V_G = -244$ mV where I_D exhibits the same time constant as for $V_G = -92$ mV which is limited by the RC time constant of the bias network in the LNA. In Fig. 6(b), the gain still recovers above noise floor within 0.5 μs but with no overshoot and slowly stabilized at similar time as I_D. In addition, the noise transient in Fig. 6(b) stabilizes with the same time constant as I_D. The difference between transient and static behavior in gain and noise for the last 10% recovery implies a longer process than seen in Fig. 6.

Since the PSD acquired by our method is wideband, the gain and noise transients can be plotted over frequency; see Fig. 7. Even though the flat-band assumption was not valid at the edge of the LNA bandwidth, the gain and noise data extracted from the 0.5-GHz averaged PSD are still informative despite some distortion. From Fig. 7(a), the gain recovery is uniform in the frequency domain for both $V_G = -92$ mV and $V_G = -244$ mV. However, the noise is observed to gradually recover its bandwidth in the frequency domain over time for $V_G = -244$ mV, illustrated in the bottom of Fig. 7(b). The bandwidth recovery progress is more significant at lower band edge and cannot be observed in the gain transients. This can be explained by the high sensitivity of the noise match at low-power bias for the HEMT and also the worse noise matching at lower frequency of the LNA design [20]. Due to its rapid recovery, the bandwidth recovery process is not captured for $V_G = -92$ mV; see the top of Fig. 7(b).

IV. Conclusion

We proposed and verified a direct method to quantitatively characterize the transient noise and gain of a pulse-operated HEMT LNA with 50-ns resolution over a wide bandwidth. This method is of interest to characterize low-power receivers system using pulsed LNAs.

References

[1] P.-J. Peng, C. Kao, C.-Y. Wu, and J. Lee, "A 79-GHz bidirectional pulse radar system with injection-regenerative receiver in 65 nm CMOS," in *Proc. IEEE Radio Freq. Integr. Circuits Symp.*, Jun. 2014, pp. 303–306.

[2] S.-Y. Jeon, K. Nikitin, A. Dewantari, J. Kim, and M.-H. Ka, "Low-noise amplifier protection switch using p-i-n diodes with tunable open stubs for solid-state pulsed radar," *IEEE Microw. Wireless Compon. Lett.*, vol. 27, no. 11, pp. 1004–1006, Nov. 2017.

[3] J. Gallimore, "Noise figure recovery measurement (microwave FET amplifiers)," in *Proc. IEE Colloq. Microw. Devices, Fundam. Appl.*, Mar. 1998, pp. 1–8.

[4] M. S. Muha, A. A. Moulthrop, and C. P. Silva, "Nonlinear noise measurement on a high power amplifier," in *Proc. 55th ARFTG Conf. Dig.*, vol. 37, Jun. 2000, pp. 1–4.

[5] Y. Z. Xiong, G.-I. Ng, H. Wang, and J. S. Fu, "DC and microwave noise transient behavior of InP/InGaAs double heterojunction bipolar transistor (DHBT) with polyimide passivation," *IEEE Trans. Electron Devices*, vol. 48, no. 10, pp. 2192–2197, Oct. 2001.

[6] J. Looney, D. Conway, and I. Bahl, "An examination of recovery time of an integrated limiter/LNA," *IEEE Microw. Mag.*, vol. 5, no. 1, pp. 83–86, Mar. 2004.

[7] C. Chambon, L. Escotte, S. Gribaldo, and O. Llopis, "*C*-band noise-parameter measurement of microwave amplifiers under nonlinear conditions," *IEEE Trans. Microw. Theory Techn.*, vol. 55, no. 4, pp. 795–800, Apr. 2007.

[8] M. Rudolph et al., "Highly robust X-band LNA with extremely short recovery time," in *IEEE MTT-S Int. Microw. Symp. Dig.*, Jun. 2009, pp. 781–784.

[9] A. Liero, M. Dewitz, S. Kuhn, N. Chaturvedi, J. Xu, and M. Rudolph, "On the recovery time of highly robust low-noise amplifiers," *IEEE Trans. Microw. Theory Techn.*, vol. 58, no. 4, pp. 781–787, Apr. 2010.

[10] O. Axelsson, N. Billström, N. Rorsman, and M. Thorsell, "Impact of trapping effects on the recovery time of GaN based low noise amplifiers," *IEEE Microw. Wireless Compon. Lett.*, vol. 26, no. 1, pp. 31–33, Jan. 2016.

[11] N. Novaris, P. Blount, and C. Trantanella, "On the measurement of pulse recovery times in gallium nitride low noise amplifiers," in *Proc. 47th Eur. Microw. Conf. (EuMC)*, Oct. 2017, pp. 580–583.

[12] A. Tomaz, S. Gerlich, M. Rudolph, and C. Andrei, "A novel system for recovery time measurements of GaN-based low-noise amplifiers," in *Proc. 14th German Microw. Conf. (GeMiC)*, May 2022, pp. 65–68.

[13] M. van Heijningen, D. C. A. Ribeiro, A. P. de Hek, and F. E. van Vliet, "Characterization of GaN recovery effects under high-power pulsed RF stress," in *Proc. 17th Eur. Microw. Integr. Circuits Conf. (EuMIC)*, Sep. 2022, pp. 37–40.

[14] J. Martens, "Noise measurements in the presence of large signal transients and studies of recovery effects," in *Proc. 100th ARFTG Microw. Meas. Conf.*, Jan. 2023, pp. 1–5.

[15] L. Boglione, "A brief walk through noise: From basic concepts to advanced measurement techniques," *IEEE Microw. Mag.*, vol. 22, no. 7, pp. 33–46, Jul. 2021.

[16] H. T. Friis, "Noise figures of radio receivers," *Proc. IRE*, vol. 32, no. 7, pp. 419–422, Jul. 1944.

[17] Low Noise Factory. (2022). *LNF4-8C Datasheet*. Accessed: Mar. 8, 2022. [Online]. Available: https://www.lownoisefactory.com/wp-content/uploads/2022/03/lnf-lnc4_8c.pdf

[18] L. Boglione, "Novel experimental determination of differential amplifier noise parameters," in *Proc. 47th Eur. Microw. Conf. (EuMC)*, Oct. 2017, pp. 656–659.

[19] J. C. Bardin, D. Sank, O. Naaman, and E. Jeffrey, "Quantum computing: An introduction for microwave engineers," *IEEE Microw. Mag.*, vol. 21, no. 8, pp. 24–44, Aug. 2020.

[20] Y. Zeng, J. Stenarson, P. Sobis, N. Wadefalk, and J. Grahn, "Sub-mW cryogenic InP HEMT LNA for qubit readout," *IEEE Trans. Microw. Theory Techn.*, vol. 72, no. 3, pp. 1606–1617, Mar. 2024, doi: 10.1109/TMTT.2023.3312471.